SAE INTERNATIONAL

ARTICLE INFO
Article ID: 04-15-03-0016

doi:10.4271/04-15-03-0016

Investigation of Water Droplet Size Distribution in Conventional and Sustainable Aviation Turbine Fuels

Judith Ugbeh Johnson,[1] Mark Carpenter,[1] Nonso Evaristus Okeke,[2] Somtochukwu Godfrey Nnabuife,[2] and Nathalie Mai[1]

[1]Cranfield Defence and Security, Centre for Defence Chemistry, Defence Academy of the United Kingdom
[2]Cranfield University, School of Water, Energy, and Environment, UK

Abstract

Water droplet size variation has been established in the literature as an important variable that influences the behavior and characteristics of water in fuel emulsion. However, with the growing demand for sustainable aviation fuels (SAF), no data is available that shows how these fuels will affect the size of dispersed water droplets and their frequency distribution. To address this lack of knowledge, this study explores and presents experimental results on the characterization of dispersed water droplets in alternative fuels and Jet A-1 fuel under dynamic conditions. The alternative fuels comprised of two fully synthetic fuels, two fuels synthesized from bio-derived materials, and one bio-derived fuel. The data and statistics presented reveal that water droplet frequency and size distribution are sensitive to changes in fuel composition. Observations showed an evident transition of the droplet percentile over time in the cumulative frequency distribution; this could be attributed to droplet coalescence to form larger droplets. Mean droplet diameters between 3 and 6 μm were observed for all the fuels tested. With further analysis based on recommendations proposed in this work, the data may assist in providing insight to filter manufacturers.

Value of Data/Highlights

- The dataset provides the aviation industry with insight into the behavior of dispersed water droplets in various commercially available sustainable aviation fuels.
- The data and statistics presented reveal that water droplet size/count distribution can be influenced by fuel composition.
- With further analysis based on recommendations proposed in this work, the standardization of test specifications can be improved.

History

Received: 24 Sep 2021
Revised: 28 Dec 2021
Accepted: 06 May 2022
e-Available: 17 May 2022

Keywords

Sustainable, Turbine fuels, Fuel systems, Aviation, Shedding, Jet fuel, Aircraft

Citation

Ugbeh Johnson, J., Carpenter, M., Okeke, N., Nnabuife, G. et al., "Investigation of Water Droplet Size Distribution in Conventional and Sustainable Aviation Turbine Fuels," *SAE Int. J. Fuels Lubr.* 15(3):2022, doi:10.4271/04-15-03-0016.

ISSN: 1946-3952
e-ISSN: 1946-3960

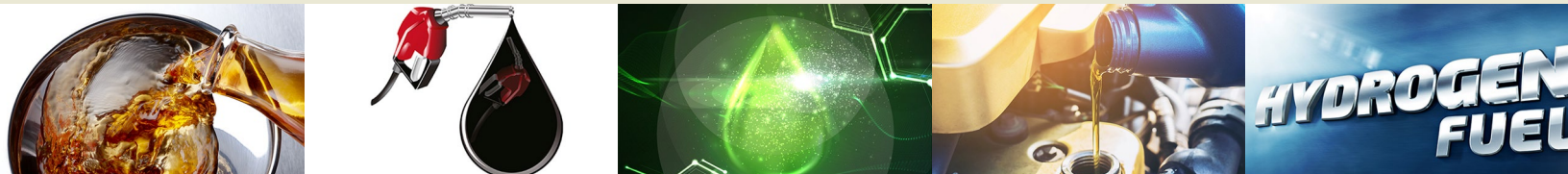

1. Introduction

Sole dependency on petroleum-derived fuels poses an increase in environmental concerns and price fluctuations [1, 2]. Hence, the revolution of sustainable aviation fuels (SAF) is featured to have the potential to decrease the life cycle of greenhouse gas emissions [3, 4, 5, 6]. These sustainable fuels are derived from renewable sources or biomass and can therefore reduce the contribution of greenhouse gas (GHG) emissions to the global climate. Alternative jet fuels could be adopted to reduce the impact of the aviation industry on air quality [7, 8].

Although alternative fuels seem like a promising technology for the aviation industry, some alternative fuels (oxygenated fuels) have high water solubility [9]. The alternative fuels available are low in sulfur and tend to be low in aromatics [10, 11, 12, 13]. Previous work has established that a low aromatics content may lead to a reduced water contamination and elastomer (seal) shrinkage, while a low sulfur content leads to lower lubricity of the fuel [13]. As a result, most SAF can be used after being blended with a certain percentage of conventionally refined jet fuel [6]. An understanding of the properties of sustainable fuels, along with the chemical properties of existing fuel types, is required to understand their impact on aircraft fuel systems.

Water uptake is one such property of interest as it is a known problem within the aviation industry [14]. An upper limit on the water content in conventional fuels is not mandated in ASTM D1655, but the expectation is that the fuel will be maintained in a clean condition and be relatively absent of free water and solid particulates; a qualitative test for free water is described in ASTM D4176 (the "Clear and Bright" test) and ASTM D3420 describes a quantitative test for undissolved water in a flowing fuel stream. The specification for jet fuels containing synthesized components is stricter on water content and requires a maximum of 75 mg/kg of total water, as assessed by Karl Fischer (KF) coulometry for ASTM D6304.

Water is said to be ubiquitous and has no calorific value. Entrained water droplets in aircraft fuel systems may result in ice formation at low temperatures, with the potential to cause an interruption of fuel flow to engines. Water may enter fuel tanks during normal flight operations like intake of moist air during aircraft descent, refueling, and routine aircraft maintenance. In jet fuel, water could exist as puddles at the bottom of fuel tanks, suspended droplets, and in dissolved form [14, 15]. Water is said to be dissolved when it exists in a molecular form and is invisible to the human eye. Dissolved water can gradually dissociate from fuel and become suspended or dispersed as tiny droplets. Dispersed water can exist in fuel when the total water content exceeds the solubility limit of the fuel at a given temperature. Free water is excess water that settles at the bottom of the fuel tank as a separate layer because water is denser than fuel [16, 17, 18]. Traditionally, dispersed or free water can be detected by looking to see if a fuel sample is clear and bright, and free from a second phase [19, 20]. Operating conditions have to be taken into consideration because the smallest possible size the unaided human eye can resolve is between 30 and 40 µm at ~200 mm from the eye. Droplets of the order of a few microns can negatively affect fuel system performance because they can freeze and accrete to form larger ice crystals, which might impede flow through filters [17]. Work by Lam et al. reported the initial sizes of suspended droplets (below 5 µm) form an emulsion with the fuel while droplets with sizes greater than 13 µm could later settle out as free water and collect at the bottom of the fuel tank or stagnation points because of their higher density [21]. The work by Clark et al. reported that free water droplets within fuel can have a diameter within the range of 20-30 µm [22]. Free water or dispersed water can be controlled by regularly draining it out from the bottom of the tank after settling [15]. This activity is referred to as "sumping" [13, 23]. Sumping is an operational maintenance procedure that is practiced to date because of the safety implications of free water in jet fuel. Yet there is no reliable data that focuses on the quantification of dispersed water droplet sizes in alternative aviation fuels (those that conform to the requirements of ASTM D7566). The study conducted by Clark et al. in 2011 quantified the droplet size and dirt count distribution exclusively in Jet A-1 fuel [22]. Clark et al. conducted experiments at ambient temperature using a process image analyzer; the result obtained identified the maximum droplet sizes to be in the range of 20-30 µm for fuel free of surfactants and below 10 µm in fuel containing low levels of surfactants. Work sponsored by the European Union Aviation Safety Agency (EASA) quantified droplet measurement over a temperature range of 10°C to −44°C using cold stage microscopy and a visual process analyzer (ViPA) [22]. The water droplet count reported in this work was shown to increase with a decrease in temperature while the sizes detected were in the range of 2-5 µm [22].

The literature has identified water solubility, total water content, size of water droplets, particulates, and temperature to predominantly influence the process of ice formation/accretion in aircraft fuel systems [13, 24, 25, 26, 27, 28, 29]. So far the effects of water solubility and temperature in sustainable and conventionally refined jet fuels have been studied from different angles, while research activities are still ongoing to develop more efficient ways to tackle the issue of water contamination in fuel. An extensive review by Goodarzi et al. deduced that a fundamental variable that influences water behavior and characteristics in fuel emulsion is the water droplet size distribution (DSD) [30]. Visual particle counting methods have been introduced in ASTM D7619-17 and ASTM D8166-21a to improve the quantification of water contamination in fuel. However, the availability of data in this research area is deficient. It has been postulated that continuous visual particle analysis will help address safety concerns and increase operational performance by improving classification (organizing generated data into relevant categories) [22, 31]. Additionally, continuous visual particle monitors may give a better insight, especially to filter manufacturers, with respect to separation processes. This work is aimed at establishing the particle size and frequency distribution of dispersed water in jet fuel by focusing on the following objectives:

- To examine the frequency size variation and count of dispersed water droplets in alternative aviation fuels under dynamic conditions.
- To demonstrate the impact of water content and time on the water droplet size and count distribution.

2. Experimental Method

2.1. Jet Fuel Characterization

The fuels were provided by Airbus for this work and were representative of both conventional and alternative jet fuels (to ASTM D7566) commercially available at the time these tests were conducted. Conventional jet fuel is defined as fuel refined principally from crude oil resources. In contrast, alternative jet fuel is identified as any fuel produced from unconventional sources. Unconventional sources include a range of energy-carrying materials which can be reprocessed either individually or in combination to yield aviation-grade fuels. Such materials include a range of hydrogen-carbon-containing materials such as biofuel, alcohols, hydrogen, coal-derived liquid fuels, and natural gas. Fully synthetic fuels are liquid fuels produced from coal, natural gas, or organic feedstocks by a gasification process, followed by Fischer-Tropsch synthesis and then conventional refining processes. Sustainable aviation fuel (SAF) is a subset of alternative jet fuel and is regarded as a fuel produced from organic feedstocks, which have absorbed carbon dioxide during growth, such as purpose-grown crops, biomass, algae, agricultural residue, or waste oils, e.g., used cooking oil and fats. The use of SAF partly mitigates the issue of global warming from aviation with a reduction in new carbon emissions compared to conventional jet fuel.

The five alternative fuels supplied by Airbus were representative of different feedstocks and processing routes that can be used to create alternative fuels; a brief summary of the fuels tested is given in Table 1. The alternative fuels contain hydrocarbons which are similar to those found in conventional jet fuels, but the range and distribution of hydrocarbon types is limited, due to the different process characteristics. Alternative fuels tend to be light in aromatics and naphthenics, which means the fuels may struggle to meet the minimum Jet A/Jet A-1 specifications for aromatics and density. However, within limits, they can be blended with conventional fuels to yield a product fit for aviation purposes. Low aromatics content in the alternative fuels compared to conventional Jet A-1 may lead to the expectation of lower water solubilisation and hold-up characteristics. However, there is a degree of interplay between the different hydrocarbon species in fuels, including the effect of hydrocarbon chain lengths, which makes water uptake in a particular fuel difficult to predict with certainty.

Fully synthetic fuels are produced by a multi-stage process. Firstly, the feedstock must be decomposed to yield syngas, a mixture of carbon monoxide and hydrogen; solid feedstocks like coal or biomass are gasified, whilst light hydrocarbon gases need to be steam reformed. The second stage is Fischer-Tropsch (FT) synthesis which involves reacting the syngas mixture at an appropriate temperature and pressure in the presence of a FT catalyst to create liquid hydrocarbons; process conditions and hydrogen to carbon ratio affect the output hydrocarbons. Finally, the product is hydroprocessed, and refined in the usual way [36][37]. The SASOL fuel was derived from coal and the FT process largely yields paraffinic hydrocarbons, i.e., a mixture of n- and iso-alkanes; hence the end product is known as synthetic paraffinic kerosene (SPK). The Syntroleum fuel was derived from natural gas, so the process is known as gas to liquid technology or GTL; like SASOL, the process tends to yield mainly paraffinic hydrocarbons.

Hydroprocessed esters and fatty acids (HEFA) is a fuel derived from fatty or oily materials of vegetable or animal origin. It is one of the most commercially viable alternative jet fuels produced from renewable feedstocks. The precursor molecules are triglycerides - three fatty acids of carbon chain lengths between C8 and C24, linked together by a glycerol backbone. Apart from pre-treatment, the main process step is hydrotreatment to break the glycerol linkage, remove oxygen and open residual double bonds. The fuel can then be refined in the normal way. Like the previous two fuels, HEFA tends to be composed of n-alkanes and iso-alkanes [38][39].

Alcohol-to-jet (ATJ) fuels are viable alternative fuels that are produced from ethanol or iso-butanol and processed by dehydration, oligomerization, hydrogenation and

TABLE 1 Summary of the characteristics of fuels used for these tests.

Fuel type	Category	Density at +15°C (kg m^{-3})	Viscosity at −20°C (mm^2 s^{-1})	Aromatics content (% v/v)
Coryton Jet A-1	Conventional fuel	796.7	3.559	17.1
SASOL FT SPK	Synthetic fuel	761	3.4	2.1
Syntroleum S-8 GTL	Synthetic fuel	756*	4.7	0.0
Honeywell HEFA-SPK	Synthetic bio-derived fuel	760	5.1	0.6
Gevo ATJ-SPK	Synthetic bio-derived fuel	759	4.8	0.5
Total Amyris farnesane	Bio-derived fuel	770	14.28	-**

* At 15.6°C.

** Not specified, but approximately zero, since farnesane is a mono-constituent fuel.

fractionation [40]. ATJ produced from iso-butanol mainly comprises of highly branched iso-alkanes of 8, 12, or 16 carbons [39]. The Gevo ATJ-SPK is produced from iso-butanol, and consists mostly of 2,2,4,6,6-pentamethylheptane ($C_{12}H_{26}$) with a lesser amount of 2,2,4,4,6,8,8-heptamethylnonane ($C_{16}H_{34}$); it does not contain significant aromatics, although it is possible to modify the process route to include an aromatisation step and create a fuel closer to the Jet A/Jet A-1 specification [38].

Unlike other SAF, farnesane (synthesized iso-paraffins or SIP) is a mono-constituent hydrogenated sesquiterpene. It is produced commercially by fermentation of sugarcane using a genetically engineered yeast to yield farnesene, a branched C15 iso-alkene with four double bonds [38][39]. Farnesene is then hydroprocessed to break the double bonds and yield farnesane; 2,6,10-trimethyldodecane. The resulting SIP fuel could contain traces of olefins and other by-products [38].

1-hexanol from Sigma Aldrich was used as a baseline for comparison with the above test cases.

2.2. Droplet Size Measurement Using the Jorin ViPA

The ViPA system selected for this experiment was manufactured by Jorin Ltd., Whetstone, Leicester, England. This unit uses a video microscope that consists of a high-speed digital video camera, a light source, and a lens. Images were analyzed in an ongoing sequence from the video system at approximately 20 frames per second; periodic data collection was specified. In this mode, images were collected and then written to memory in brief bursts to monitor the size distribution trend in real time. The flow through the cell was maintained at a constant rate to ensure that droplets were not counted more than once. The continuous data were accumulated for 1 hour and reported as counts per 39 s.

3. ViPA Data Analysis

The objective of this study was to characterize the effects of water concentration and homogenization conditions on the DSD, droplet count, frequency distribution, and estimated volume in different fuels.

A set of user-defined parameters were entered into the ViPA, enabling the system to discriminate between various classes of particles (based on shape, size, and opacity). The system can calculate data on several classes of measured parameters, but in the present study, size, shape factor (SF), visible water concentration, and volume were analyzed. For the size parameter, the system measures particle diameter in a specified direction between two parallel tangential lines and reports it as the mean of the measured Feret diameter. For each object, the ViPA measures four diameters, which are known as Feret diameters, at fixed angular intervals. The average droplet sizing for this work is defined as the summation of the diameter "d" of droplet size from "i" equals 0 to ∞ (number of imaged particles) then divided by the summation of the total number of frames or total frequency of occurrence (n).

The flow cell channel is approximately 6 mm wide × 2 mm deep; at a volumetric flow rate of 20 mL/min, this gave a linear flow of 27.8 mm/s. Images were captured at regular intervals (20 frames per second) and sent to the computer for analysis. The image captured by the system is 1024 × 778 pixels with a pixel size of 0.47 µm. This equates to a field of view of 481 × 366 µm; the depth of field is 300 µm, which gives an assessed fluid volume of 52.8×10^6 µm^3. In practical terms, the VIPA is able to detect particles up to 250 µm across.

To determine if a particle is round (spherical water droplet or gas bubble), a minimum of 3 adjacent dark pixels are required in a 3 × 3 grid. When an object is smaller than 1.5 µm, the system cannot determine sphericity and the particle is assumed to be a hard solid. The software interprets what is a valid object and what is not using two parameters: "Edge strength" and "Threshold". The "Edge strength" is a measure of the object being in focus; an object in focus will appear with well-defined edges. "Threshold" defines the different tones (256 gray levels) possible on the gray scale. This gives the software the ability to differentiate between objects of interest, which tend to obscure light and therefore appear darker gray, and the background fuel, which appears pale gray. Water droplets in jet fuel generally appear to be circular with a dark perimeter and brighter center, while hard particulates tend to be more angular and will appear to be uniformly dark.

The De Brouckere mean diameter was selected for this work because the distribution calculated takes volume and mass into account [35, 36]. The De Brouckere mean diameter is the weighted volume average (WVA) of a particle size distribution. The equation for the average droplet sizing $\underline{D}_{1,0}$ and weighted-volume average $\underline{D}_{4,3}$ can be written as

$$\underline{D}_{[1,0]} = \frac{\sum_{i=0}^{\infty} n_i d_i}{\sum_{i=0}^{\infty} n_i} \qquad \text{Eq. (1)}$$

$$\underline{D}_{[4,3]} = \frac{\sum_{i=0}^{\infty} n_i d_i^4}{\sum_{i=0}^{\infty} n_i d_i^3} \qquad \text{Eq. (2)}$$

The key parameter that enables the system to discriminate between objects is the SF. Mathematically, the shape factor for any class of object is represented as SF = 4π Area/Perimeter^2. In principle, the SF is inversely proportional to the perimeter; therefore, for a given area, an increase in the perimeter decreases the SF. The system defines a spherical SF to be within the range of 0.9-1 and a square as 0.75. The visible water concentration in parts per million (ppm) is principally analyzed based on the focal volume. Therefore, the concentration assumes that the volume of fluid passing through the flow cell is sufficient that, for every frame captured, a fresh volume of fluid is analyzed. Concentrations are not absolute but have been proved to be statistically reliable. However, the visible parts per million (Vppm) has been proved to be a representation of changes to measurements over time [31]. Finally, the

estimated volume of water droplets is mathematically represented as the volume of a sphere ($4/3\pi r^3$).

Results obtained for size distribution are presented in histograms/distribution curves showing the frequency and size distribution for a given set of test conditions. Another way the DSD result was presented was by calculating the kurtosis and skewness for all test cases. The kurtosis and skewness provide more statistical evidence [37]. The equations used for calculating skewness and kurtosis are given by

$$\text{Skewness}\,(sk) = \frac{n}{(n-1)(n-2)}\sum_{i=1}^{n}\left(\frac{di-\underline{d}}{s.d.}\right)^3 \quad \text{Eq. (3)}$$

$$\text{Kurtosis}\,(k) = \frac{n(n+1)}{(n-1)(n-2)(n-3)}\sum_{i=1}^{n}\left(\frac{di-\underline{d}}{s.d.}\right)^4 - 3\frac{(n-1)^2}{(n-2)(n-3)} \quad \text{Eq. (4)}$$

where *s.d.* is the standard deviation and $\underline{d}$ the mean droplet size diameter.

Kurtosis relates to the "tailedness" of the probability distribution of a real-valued random variable' and how the data corresponds to the greater effect of outliers. For a standard normal distribution, the value of kurtosis is 3. Statistically, the skewness measures the lack of symmetry of a dataset. The skew parameter tends to be negative mostly when a secondary peak at a high diameter is present in the distribution (small droplets colliding to form large droplets can lead to such secondary peaks).

3.1. Preparation of Dispersed Water in the Jet Fuel Mixture

A volume of 100 mL of fuel was prepared in a 100 mL measuring cylinder (approximately 32 mm diameter) to allow a reasonable height for the rate of water settling to be analyzed. The emulsion was prepared by adding a measured amount of distilled water (0.1% w/w of water) to the fuel at approximately 19°C and blending with an X 620 high shear mixer.

All water content measurements reported in this article were conducted by KF coulometry using a Metrohm 831 KF coulometer; this unit was fitted with a generator electrode with diaphragm. The titration vessel was filled with Hydranal Coulomat AG-H solution. It is noteworthy that, as received, all fuels were below the maximum acceptable total water content of 75 ppm (for fuels that comply with ASTM D7566) before the water addition. Table 2 summarizes the fuel mixtures prepared. The "Case a" tests examined the effects of the fuel composition.

The image of the experimental setup is shown in Figure 1. The fluid was sheared by a high-speed revolving impeller; the shearing effect is proportional to the impeller speed. For these

TABLE 2 Summary of "Case a" test fuels. In each case, 0.1% water addition was made; the water was dispersed with a high shear mixer.

Test cases	Fuel	Fuel type/category
Case a.1	Coryton Jet A-1	Conventional fuel
Case a.2	SASOL	Synthetic fuel
Case a.3	GTL S-8	Synthetic fuel
Case a.4	HEFA	Synthetic bioderived fuel
Case a.5	ATJ	Synthetic bioderived fuel
Case a.6	Farnesane	Bio derived fuel

tests, the emulsion was homogenized for 60 s at a constant speed of 11,000 RPM.

After the preparation of the emulsion, the "inlet" flow line (blue flexible tube in Figure 2) was placed in the middle of the measuring cylinder while the "outlet" flow line was placed in an empty beaker. At this point, the peristaltic pump was started to allow approximately 2 mL to flush through the system to coat the inside of the flow line and eliminate any air trapped in the system. Subsequently, software analysis was started, and the open end of the "outlet" flow line was located at the bottom of the measuring cylinder (orange flexible tube in Figure 2). This procedure ensured that the emulsion retains the dispersed water droplets as some fuels tend to shed water fractions quickly depending on their level of hydrophobicity, or the presence of polar compounds.

Immediately after starting the ViPA system, a snapshot and a video were taken for visual comparison of the water

FIGURE 1 X 620 high shear mixer used for water dispersion.

FIGURE 2 Experimental setup used for suspended water droplet size analysis.

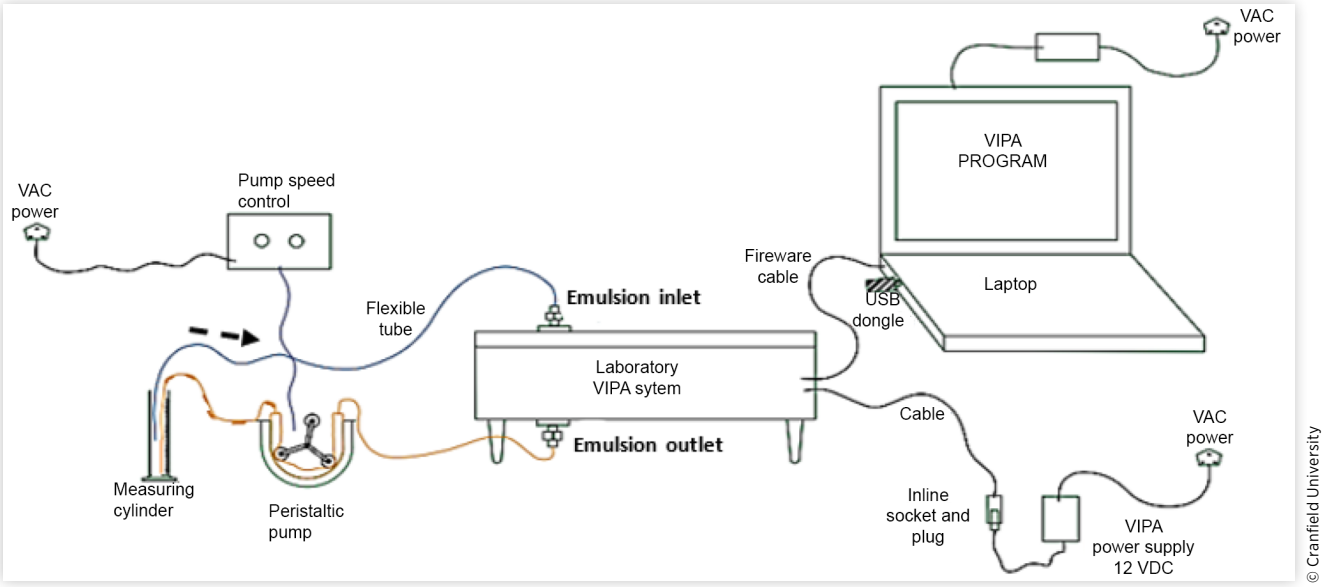

droplet size at the beginning and end of an experiment run. The experimental setup is shown schematically in Figure 2.

An initial water content analysis was conducted using KF coulometry a few minutes after mixing the emulsion, and then at intervals through each test; the KF tests adopted the procedure given in ASTM D6304. The KF results are shown in Table A.1, Appendix A.

4. Results and Discussion

4.1. ViPA Data Analysis

The ViPA is capable of continuous image analysis of small objects within its field of view—the fuel/water mix in this case. This study aimed to characterize dispersed water droplets which, in principle, are spherical because of surface tension effects; such droplets will have an SF between 0.9 and 1. As the visual analyzer assigns a given size to each water droplet, the main operations carried out to obtain the size distributions are predefining droplets properties and contours, image acquisition, and statistical analysis. The experiments conducted in this work addressed the influence of (1) fuel composition and (2) total water content on the size distribution of water droplets. Table 3 summarizes the results from the ViPA data analysis for Test cases a.1 to a.6. The SF for these test cases was well within the range of 0.9-1, indicating that the detected droplets were spherical. The uncertainty of the arithmetic mean diameter is 5% at a 95% confidence level for every measurement.

In use, the video system operates at 20 frames per second. It performs a background calibration of 100 frames and then a burst of 361 frames in image analysis mode. From the frame rate, it can be deduced that the instrument makes measurements for 18.05 s within each imaging cycle. Each particle that is identified by the software is measured and aggregate statistics recorded in spreadsheet form. On completion of an imaging cycle, the data are stored in a hard disk drive and the sequence repeated. Each cycle takes 39 s and, for the purposes of this investigation, the instrument was run continuously for 1 hr for each test case.

Table 3 shows the average of the chosen parameter (size, shape, and count) for all the images captured at different time intervals. The count for all fuel samples reduces dramatically over time. This is due to recirculation of the liquid stream that creates turbulence that favors the coalescence of water droplets to larger droplets resulting in settling. Also, from Table 3, a slight drop in the WVA over time can be seen while there is a slight unstable increase in the average droplet diameter with time. However, it is noteworthy that even though Case a.6 exhibited the second highest mean diameter of 4.20 µm, it had the lowest average count of 5400 and lowest WVA of 10.36 μm^3. Also, Case a.5 exhibited the lowest mean size of 3.97 µm, yet it had the highest WVA of 12.6 μm^3 and a count of 9200. This shows that there is a relationship that exists between the water droplet size, count, and droplet volume concentration. The following sections help shed light on these correlations and expatiate on the test results for Cases a.1 to a.6.

4.2. Effects of Fuel Composition

Jet fuel does not have a particular chemical composition but is a complex mixture that is mainly specified according to physical characterization as investigated and reported by a few studies [38]. So far, it has been established that fuel properties can be directly affected by chemical composition.

TABLE 3 Suspended water droplet summary data for Test cases a.1 to a.6.

Test case	a.1	a.2	a.3	a.4	a.5	a.6
Summary result after 1 hr						
Arithmetic mean diameter $D_{[1,0]}$ (μm)	4.15	3.73	4.36	4.0	3.97	4.20
Weighted-volume average $D_{[4,3]}$ (μm)	10.46	10.67	10.86	11.68	12.6	10.36
Average count after 1 hr	15,876	14,365	17,058	12,113	9285	5424
Shape factor	0.92	0.92	0.91	0.91	0.92	0.91
Time history of particle characterization (arithmetic mean size, μm)						
39 s	4.02	3.65	4.16	3.82	3.48	4.13
1170 s	4.09	3.66	4.37	4.0	3.94	4.13
2340 s	4.18	3.76	4.28	3.98	4.08	4.23
Time history of particle characterization (weighted volume average size, μm)						
39 s	10.85	11.45	12.52	13.55	14.88	9.84
1170 s	10.67	10.68	11.32	12.1	13.02	10.36
2340 s	10.32	10.54	13.72	11.23	12.27	10.31
Time history of particle characterization (droplet count)						
39 s	20,000	18,900	16,400	18,000	17,000	9000
1170 s	10,200	14,500	10,500	12,000	8000	5000
2340 s	7500	11,000	7500	9000	6000	3300

However, with the growing demand for SAF, understanding the effect of chemical composition has become a vital topic of interest as it could potentially assist in accelerating the fuel approval process as well as providing information for fuels additive companies and filter manufacturers. This is why the water DSD of SAF was evaluated in comparison to Jet A-1 fuel in this work. The influence of chemical composition on the rate of droplet count can be seen in Figure 3(a). The time it takes the dispersed water droplets to drop out of the fuel/water mixture is a measure of the settling rate/profile. Data in Figure 3(a) illustrate the settling profile of the different fuels. Reported recent work compared the settling profile of SAF and conventional jet fuel and found the rate to decrease with time [13, 39]. Qualitatively, it is anticipated that the water separation ability can be directly influenced by the droplet size and droplet coalescence. From Figure 3(a), it can be seen that the droplet counts decrease with time and that all fuels tend to exhibit a steady exponential decay over time. This mirrors previous work by West et al. that showed that the water settling rate steadily decayed over time for both conventional and SAF [10]. In context, the rate of decay of droplet counts may be attributed to droplet coalescence [41, 42]. Evidence that will indicate that droplet coalescence was occurring is in Figures 3 and 4, showing a plot of water droplet diameter represented by 10%, 20%, 50% to 90%, or d10, d50, and d90.

As illustrated in Figure 3(a), the rates of droplet count decay are different for all the fuels; fuel Case a.6 showed the least tendency to form and suspend individual water droplets, and the slowest settling rate of all the fuel/water mixes. However, fuels with higher settling rates and a good separation ability are beneficial to the aviation industry as most aircraft fueling systems utilize filter coalescers. Since Case a.6 exhibits poorer separation ability, it can be concluded that there was good mixing of the fuel/water solution and that most of the water molecules likely dissolved in the solution. This explains the high water content value in the KF result shown in Table A.1, Appendix A; this could mean that Case a.6 has the lowest level of hydrophobicity compared to other fuels, or possibly contain more traces of polar compounds. To elucidate this point on settling behavior, the average total droplet count data were plotted for the different fuels in Figure 3(b). The ViPA detected an average count of about 15,500 after 60 min for Case a.1 with 1000 ppm water addition using a high shear mixer for water dispersion. Under the same test conditions as Case a.1, the GTL S-8 synthetic fuel employed for Case a.3 exhibited similar behavior; the ViPA system detected an average count of 17,000 after 60 min. Count data for Test cases a.1 to a.6 showed a steady decrease in droplet count in the order of a.3 > a.1 > a.2 > a.4 > a.5 > a.6.

The water solubility in jet fuel is predominantly dependent on the fuel composition, aromatics content among other factors. While the water droplet diameter, density, and dynamic viscosity can affect the settling rate/rate of drop out of precipitated droplets in fuel. Case a.6 showed the slowest settling rate and lowest droplet count; this is a bio-derived fuel with very low aromatics content and the highest viscosity, as noted in Table 1. Pathway analysis by Zschocke et al and a GC/MS characterisation by Pires et al suggests that farnesane could contain traces of unsaturated hydrocarbons (olefins) [1] [38]. Olefins contain one or more double bonds, that consist

FIGURE 3 Water droplet count with error margin (a) settling profile for Cases a.1 to a.6; (b) Average droplet count histogram data for Cases a.1 to a.6; (c) Repeatability droplet counts data for Cases a.1 and a.6.

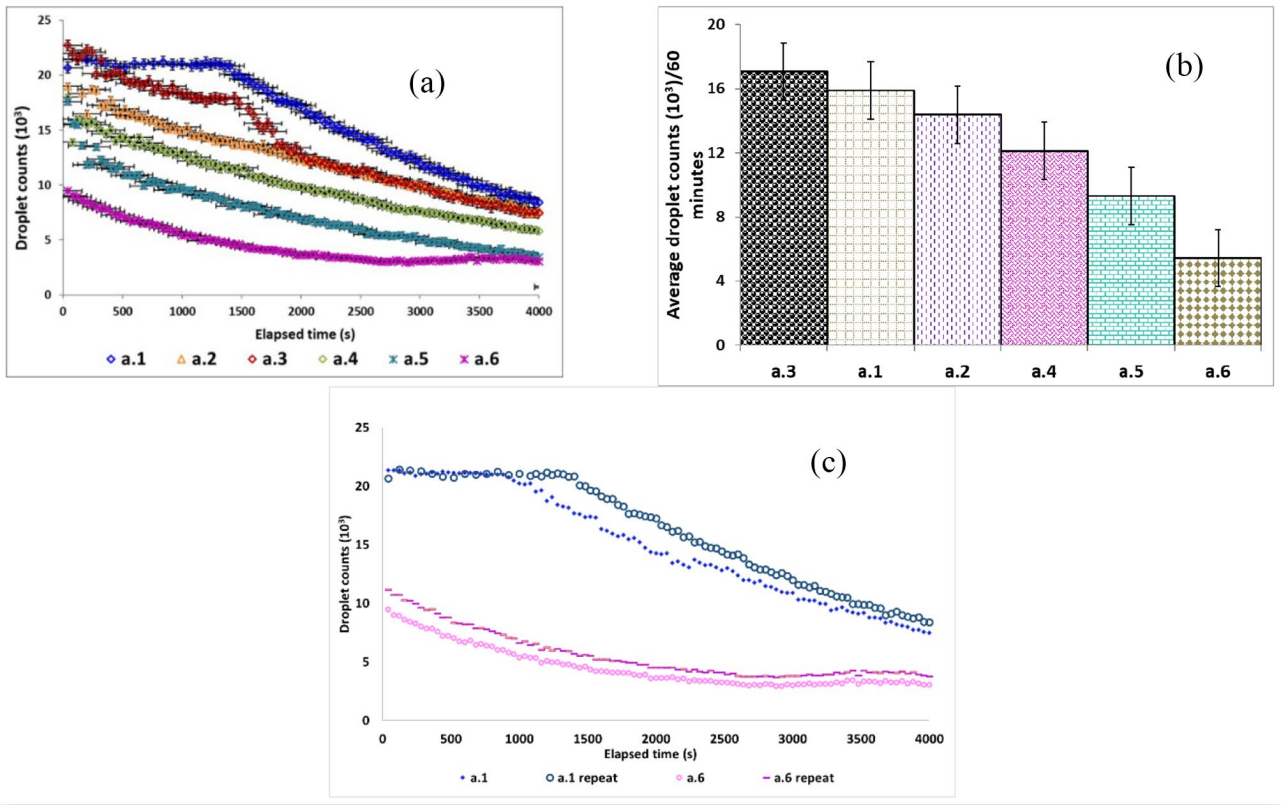

of one sigma bond and one pi bond, and therefore may contribute to slightly enhanced uptake of water. Literature has established that viscosity plays a key role in the behavior of droplets in a suspension. According to Stokes' law (which is an expression that describes the resisting force on a particle moving through a viscous liquid), the terminal velocity of a water droplet is directly proportional to the square of the droplet diameter and the density difference between fuel and water, and inversely proportional to the dynamic viscosity of the fuel [13]. Figure 4 shows the shift in the corresponding water droplet size population against time for Cases a.1-a.6.

The shift in the cumulative frequency can be used to describe the transition of the percentile of droplets over time (up to t = 4000 s). For instance, 10%, 50%, and 90%, or d10, d50, and d90, are represented as water droplet diameters equal to or below the corresponding diameter of that percentile. The water droplet size population represented from d10 to d90 against time for Test cases a.1-a.6 is shown in Appendix C (Figure C.1).

It can be seen from Figure 4 that the majority of the detected water droplets were between 2 and 4 µm. Droplet counts decrease with time because of droplet coalescence which causes an incremental shift of the d70-d90 populations at different times. This is consistent with the relationship shown in Figure 5 (illustrating the mean droplet size for all fuels with time as a variable). It can also be deduced from the cumulative frequency curve in Figure 4 that droplet sizes between d40 and d10 are likely to remain suspended in the fuel/water mixture as no settling was noticed. No noticeable change was detected with time for Case a.6 compared to other test cases.

It can be elucidated from Figure 4 that droplet size does not conform to the same pattern as droplet count. To explain this point, Case a.6 (farnesane) with the lowest droplet count of all the cases explored (Figure 3) maintained the lowest WVA over time [Figure 5(a)]. However, it exhibited a larger average droplet size over time than Cases a.1, a.2, a.4, and a.5 [Figure 5(b)]. Case a.3 (GTL S-8) showed the highest average droplet count and droplet sizes over time but did not have the highest droplet volume concentration (WVA). Previous work in this area suggests that the rate at which water droplets will fall out of a solution is dependent on the droplet volume concentrations and the square of the diameter [10]. Figures 3 and 5 shed light on the relationship that exists among the water droplet size, count, and droplet volume concentration.

It is noticeable from Figure 5 that the behavior of water droplets in hydrocarbons is often complex, and random as evidenced by a slight increase in the average droplet size with time [Figure 5(b)]. However, a noticeable drop in the water droplet volume over time can be seen in Figure 5(a). This demonstrates that the contribution from larger droplets or high-frequency counts of smaller droplets could all influence

FIGURE 4 Water droplet size population with respect to time for each fuel for Cases a.1-a.6.

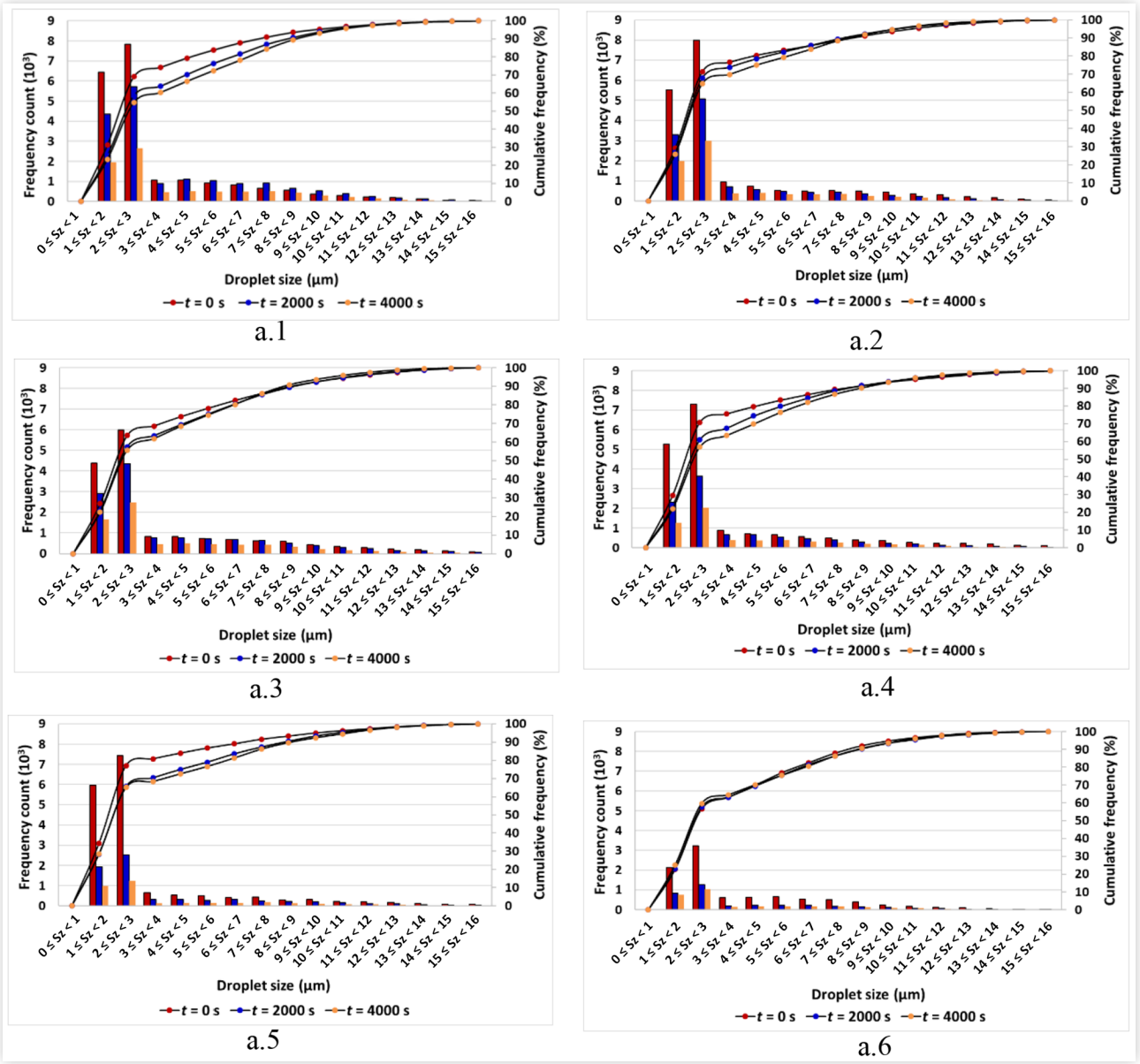

the droplet volume. A high droplet count does not necessarily correspond to a high droplet volume and, similarly, a fuel that contains few but larger water droplets do not necessarily signify that the volume will be high. The volume concentration is principally based on the mass equivalent as there could be a high-water count with small droplet sizes or a low water count with large droplet sizes. For instance, even though Case a.6 (farnesane) contained large water droplets, it had the lowest droplet volume. In addition, it had the lowest count of water droplets, while Case a.5 (ATJ) had a higher WVA because it contained a higher proportion of larger droplets. It is worth noting that Cases a.2 (SASOL) and a.1 (Jet A-1) do not have the highest droplet volume [Figure 5(a)], but they both have the highest frequency of smaller droplets compared to all other fuels, as shown in Figure 6(a).

The frequency distribution for each test in Figure 6(a) presents the droplet counts separated into discrete size intervals between Jet A-1 fuel and the SAF explored for this work. The height of the distribution peak indicates the total count of water droplets for each size range. Figure 6(a) shows that the mode droplet count frequency for all fuels explored fell within the droplet interval of 2 to 3 µm. Case a.1-Jet A-1 and Case a.2-SASOL exhibited the highest frequency of smaller droplets ranging from 1 to 3 µm.

Figure 6(b) shows the droplet count for each class of droplet size over time. Starting with Case a.6, the gradual slope for farnesane confirms that the settling rate of droplets is low compared to the other fuels. This implies that the farnesane formed a more stable emulsion relative to other fuel types. The result correlates with data from a study by Leiva

FIGURE 5 Shows the (a) WVA data against time; (b) Arithmetic mean droplet size against time for Test cases a.1 to a.6; (c) Repeatability data for arithmetic mean droplet size against time for Test case a.2; (d) Repeatability data for arithmetic mean droplet size against time for Test case a.6.

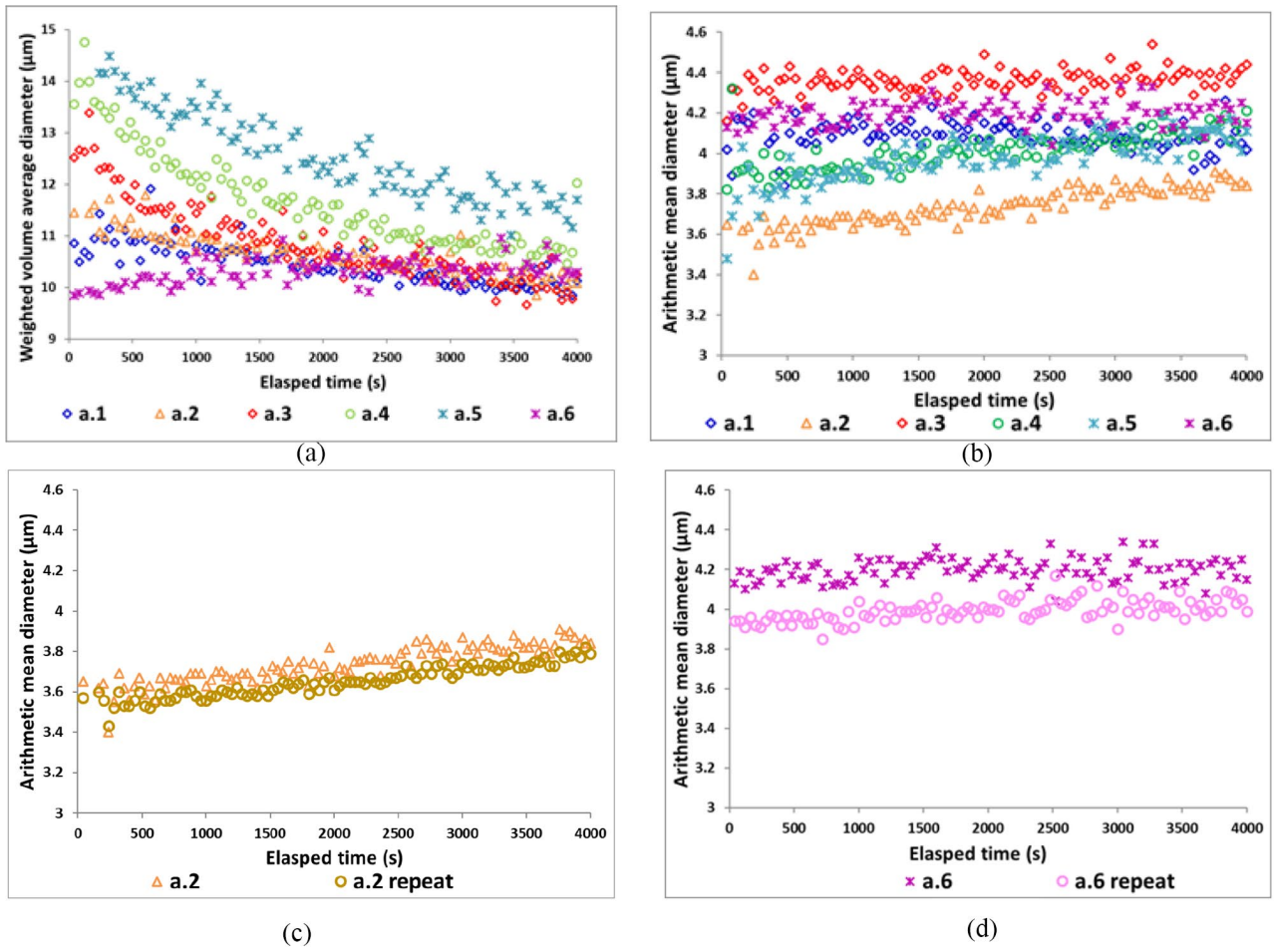

FIGURE 6(a) Frequency distribution of water droplet sizes for aviation fuels explored in this work (Cases a.1 to a.6).

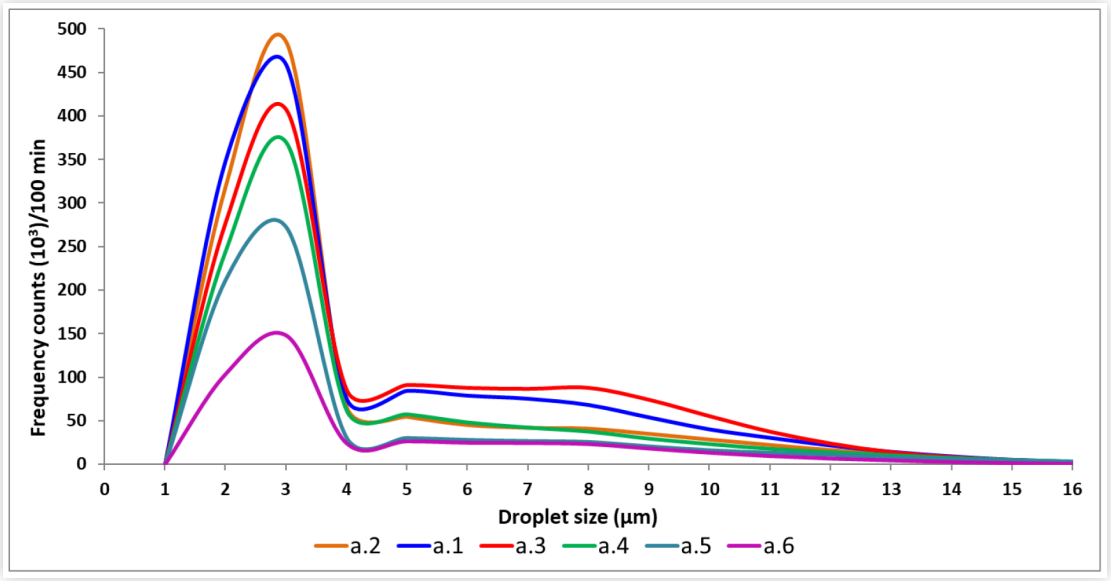

FIGURE 6(b) Comparative analysis of the frequency distribution between Jet A-1 fuel and SAF explored for this work (Cases a.1 to a.6).

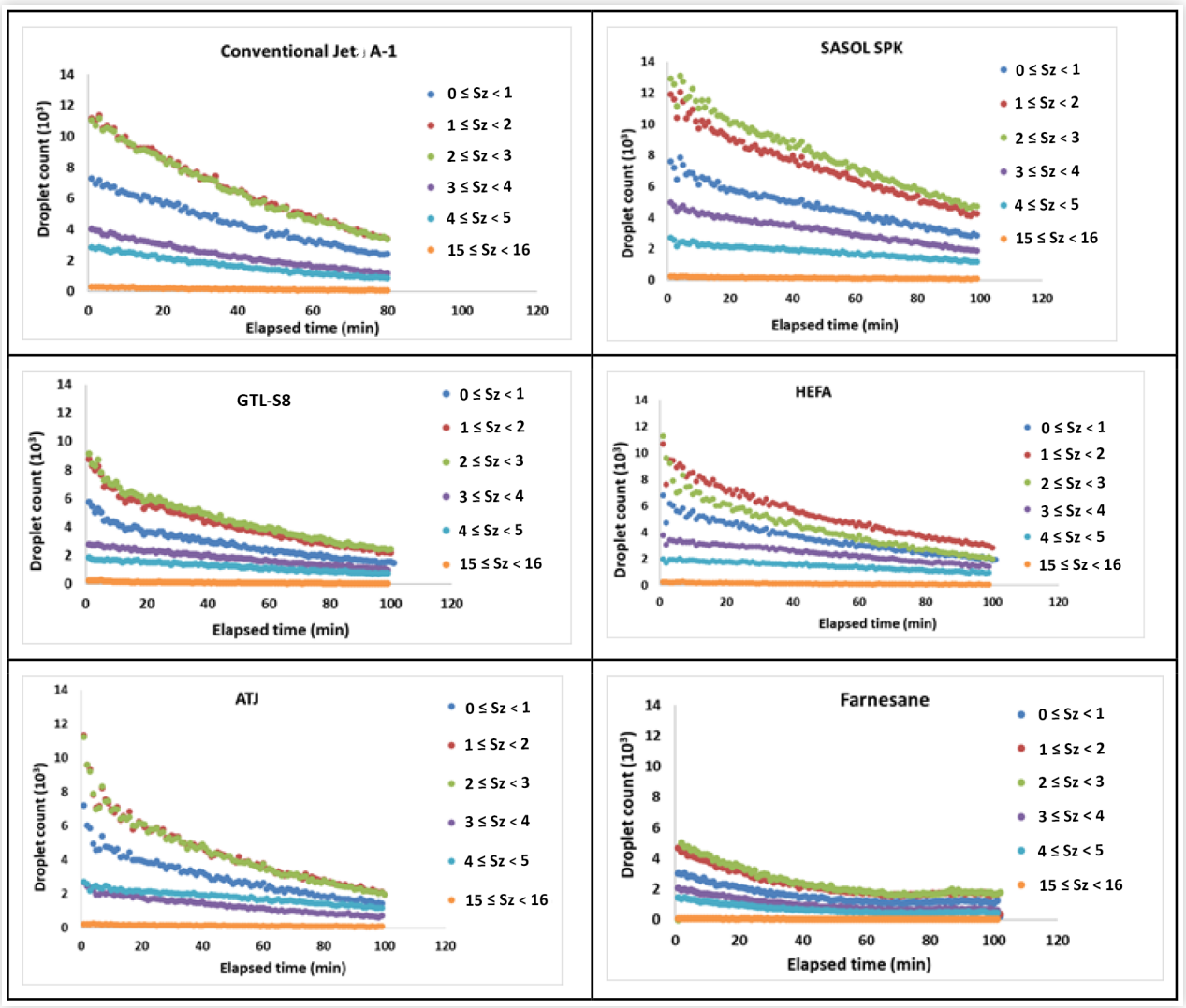

et al. on the expected behavior of emulsions and the changes in their DSD [42]. Figure B.1 in Appendix B shows a comparative analysis of the frequency distribution between Jet A-1 fuel and the SAF explored for this work.

To illustrate the appearance and distribution of water droplets in different fuels, Figure 7 shows typical images captured from the ViPA software near the start and finish of each experimental run. The images help with the visualization of the reduction in water droplet populations seen in the frequency distribution data in Figure 6(a), where water droplets disappear over time due to settling.

The size distribution plots in Figures 7a.1″-a.6″ show the droplet size increases with time due to the coalescence phenomenon—the collision of large and small drops giving rise to larger droplets. For instance, the possible interpretation for this distribution observed in Figure 7a.3″ is because of the collision of droplets with one large peak denoted as "e" centered around a 2-3 µm diameter, giving rise to larger droplets (smaller broadband denoted as "f" around 6-8 µm diameter). The same phenomenon dominates in all cases; however, in some cases, the peaks are smaller and almost insignificant. For example, Case a.6 has only one evident narrow peak denoted as "k" around 3 µm and a tiny peak denoted as "l" around 5 µm. Overall, the larger the droplets formed due to the collision of small droplets the more unstable the emulsion is (typified by Figures 7a.1″ and a.3″). DSD data for Test cases a.1 to a.6 exhibit an unstable emulsion in the order of a.3 > a.1 > a.4 > a.2 > a.5 > a.6. This result correlates with work done by Noor et al. on the stability of water in diesel fuel emulsions, concluding that the more stable an emulsion is, the narrower the DSD [41]. While this is based on the result and trend observed, the statistical evidence based on the

FIGURE 7 Images captured from the ViPA software. Column 1 (left) shows the appearance of water droplets in the fuels, 2 min after the start of each experiment. Column 2 (center) shows the appearance after 60 min of circulation/settling. Column 3 (right) shows the smoothed water DSD after 100 min.

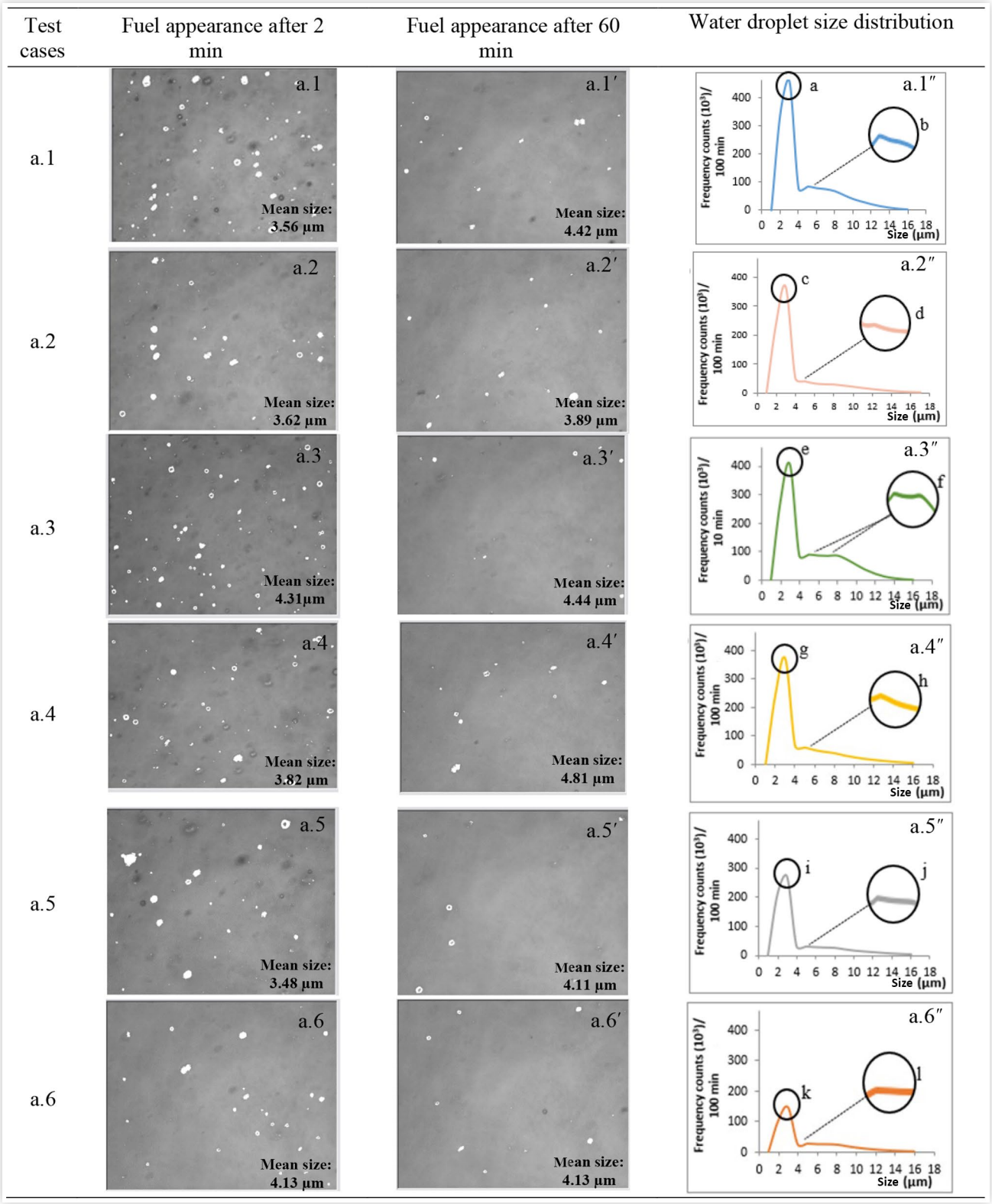

TABLE 4 Kurtosis and skewness data for Case a.1 to Case a.6.

	Case a.1	Case a.2	Case a.3	Case a.4	Case a.5	Case a.6	Hexanol
Kurtosis (after 40 min)	6.6	6.66	6.29	6.58	8.21	7.09	28.4
Skew (after 40 min)	2.63	2.79	2.65	2.75	2.95	2.68	4.6
Kurtosis (after 60 min)	7.4	7.3	7.5	7.8	10.31	9.47	34.90
Skew (after 60 min)	2.86	2.87	2.87	2.89	3.17	3.01	5.07

calculation of the kurtosis and skewness (Equations 3 and 4) further elucidates the result from the droplet distribution (Table 4).

The more unstable a solution the lower the skew value. In contrast, kurtosis relates to a metric indicating the "tailedness" of the probability distribution of a real-valued random variable and how the data corresponds to the greater effect of outliers. 1-Hexanol (which is likely to form a stable solution) was included to serve as a baseline for comparison between a stable solution and unstable emulsion and has the highest kurtosis and skew value of the fluids investigated.

The skew to the right, seen in the droplet distribution in Figures 7a.1″ to a.6″, shows that all fuels exhibit a positive skewness as the right-hand tail is longer than the left. The DSD for Cases a.5 and a.6 are characterized by their smaller secondary peaks at larger droplet sizes and slightly higher kurtosis values of 8.21 and 7.09, respectively (Table 4). DSD for Cases a.1 to a.4 is characterized by their almost evident second peak distributions and lower kurtosis values of 6.6, 6.7, 6.29, and 6.58, respectively (Table 4).

5. Conclusions and Recommendations

The fundamental variable that influences the characteristics of an emulsion in aviation fuels is the water DSD. The experimental test data has indicated that water droplet size/count distribution is sensitive to changes in fuel composition; the evaluated synthetic jet fuels, GTL S-8, SASOL, and HEFA, exhibited good water separation comparable to conventional jet fuel. This is consistent with previous work conducted on the water settling ability of various jet fuels [4, 10, 24]. Fuel with a higher water settling rate is beneficial for aviation refueling purposes. The synthetic fuels had higher droplet counts and lower skew and kurtosis values compared to the biofuels, which means good prospects for faster water separation. In contrast, the bio-jet fuels explored for this work, ATJ and farnesane, exhibited worse water separation.

Further work should be carried out at different blending ratios of sustainable fuels and temperatures (cold temperatures to simulate high altitudes). This would assist with the development of a mathematical relationship to predict the relationship that exists among the droplet size, droplet count, and droplet volume. Finally, experiments should be repeated on a larger scale with the outlet emulsion transferred to a waste container instead of the bottom of the tank/measuring cylinder.

Funding Sources

This work was funded by EPSRC-UKRI (Reference ID: 246196) and Airbus Operations, Filton, Bristol (Reference ID: 1100152106), United Kingdom.

Availability Statement

The data that support the findings of this study are openly available in Cranfield Online Research Data (CORD) repository at https://doi.org/10.17862/cranfield.rd.19027403.

Acknowledgment

The authors will like to thank Airbus Operations in Filton Bristol, United Kingdom, for the financial and relentless support toward this work.

Contact Information

J.ugbeh@cranfield.ac.uk

Definitions/Abbreviations

AFS - Aircraft fuel systems

ATJ - Alcohol to jet fuel

DSD - Droplet size distribution

ASTM D6304 - "Standard Test Method for Determination of Water in Petroleum Products, Lubricating Oils, and Additives by Coulometric Karl Fischer Titration"

ASTM D7566 - "Standard Specification for Aviation Turbine Fuel Containing Synthesized Hydrocarbons"

ASTM D7619 - "Standard Test Method for Sizing and Counting Particles in Light and Middle Distillate Fuels, by Automatic Particle Counter"

ASTM D8166 - "Standard Test Method for Sizing and Counting Particulates in Middle Distillate Fuels and Biodiesel Blend (B6 to B20) Using Continuous Flow and Bottle Sampler Automatic Particle Condition Monitors"

GHG - Greenhouse gas

GTL - Gas to liquid

HEFA - Hydroprocessed esters and fatty acid

HSM - High shear mixer

KF - Karl Fischer

RPM - Revolutions per minute

SAF - Sustainable aviation fuel

SASOL - **S**uid-**A**frikaanse **S**teenkool-, **Ol**ie- en Gasmaatskappy—South African Synthetic Oil

WVA - Weighted volume average

References

1. Pires, A.P.P., Han, Y., Kramlich, J., and Garcia-Perez, M., "Alternative Jet Fuel Properties," *BioResources* 13 (2018): 2632-2657.
2. ElGalad, M.I., El-Khatib, K.M., Abdelkader, E., El-Araby, R. et al., "Empirical Equations and Economical Study for Blending Biofuel with Petroleum Jet Fuel," *J. Adv. Res.* 9 (2018): 43-50, https://doi.org/10.1016/j.jare.2017.10.005.
3. McCoy, A.C., Duran, M.J., Azad, A.M., Chattopadhyay, S. et al., "Performance of Sulfur Tolerant Reforming Catalysts for Production of Hydrogen from Jet Fuel Simulants," *Energy and Fuels* 21, no. 6 (2007): 3513-3519, https://doi.org/10.1021/ef070111k.
4. Nygren, E., Aleklett, K., and Höök, M., "Aviation Fuel and Future Oil Production Scenarios," *Energy Policy* 37 (2009): 4003-4010, https://doi.org/10.1016/j.enpol.2009.04.048.
5. Blakey, S., Lucas, R., and Christopher, W.W., "Aviation Gas Turbine Alternative Fuels: A Review," *Proc. Combust. Inst.* 33 (2011): 2863-2885, https://doi.org/10.1016/j.proci.2010.09.011.
6. Hari, K.T., Yaakob, Z., and Binitha, N.N., "Aviation Biofuel from Renewable Resources: Routes, Opportunities and Challenges," *Renew. Sustain. Energy Rev.* 42 (2015): 1234-1244, https://doi.org/10.1016/j.rser.2014.10.095.
7. Yilmaz, N. and Atmanli, A., "Sustainable Alternative Fuels in Aviation," *Energy* 140 (2017): 1378-1386, https://doi.org/10.1016/j.energy.2017.07.077.
8. Hileman, J.I., Ortiz, D.S., Bartis, J.T., Wong, H.M. et al., *Near-Term Feasibility of Alternative Jet Fuels* (Santa Monica, CA: RAND, 2009). http://www.atac.ca/web/images/atac/files/Members_Only/Les_Alders/Technical_Operations_Engineering_Maintenance/Issues/2010_AGM_-_altfuelfeasrpt_.pdf.
9. Gutiérrez-Antonio, C., Gómez-Castro, F.I., de Lira-Flores, J.A., and Hernández, S., "A Review on the Production Processes of Renewable Jet Fuel," *Renew. Sustain. Energy Rev.* 79 (2017): 709-729, https://doi.org/10.1016/j.rser.2017.05.108.
10. West, Z.J., Yamada, T., Bruening, C.R., Cook, R.L. et al., "Investigation of Water Interactions with Petroleum-Derived and Synthetic Aviation Turbine Fuels," *Energy and Fuels* 32 (2018): 1166-1178, https://doi.org/10.1021/acs.energyfuels.7b02844.
11. Baena, S., Lam, J., and Lawson, C., "Effects of Ice Accretion in an Aircraft Protective Mesh Strainer of a Fuel Pump," SAE Technical Paper 2015-01-2449, 2015, https://doi.org/10.4271/2015-01-2449.
12. Lam, J.K.W., Carpenter, M.D., Williams, C.A., and Hetherington, J.I., "Water Solubility Characteristics of Current Aviation Jet Fuels," *Fuel* 133 (2014): 26-33, https://doi.org/10.1016/j.fuel.2014.04.091.
13. Ugbeh Johnson, J., Carpenter, M., Williams, C., Pons, J.-F. et al., "Complexities Associated with Nucleation of Water and Ice from Jet Fuel in Aircraft Fuel Systems: A Critical Review," *Fuel* 310 (2022): 122329, https://doi.org/10.1016/j.fuel.2021.122329.
14. Baena, S., Repetto, S.L., Lawson, C.P., and Lam, W., "Behaviour of Water in Jet Fuel—A Literature Review," 60 (2013): 35-44.
15. Chan, K.Y. and Lam, J.K.-W., "Water Drop Runoff in Aircraft Fuel Tank Vent Systems," *J. Mech. Eng. Sci.* 23 (2016): 4548-4563, https://doi.org/10.1177/0954406216669175.
16. Naya, S., Cao, R., Francisco-Fernández, M., Tarrío-Saavedra, J. et al., "Estimating Water and Solid Impurities in Jet Fuel from ISO Codes," *Energy and Fuels* 27 (2013): 7858-7867, https://doi.org/10.1021/ef401378z.
17. Maloney, T.C., Diez, F.J., and Rossmann, T., "Ice Accretion Measurements of Jet A-1 in Aircraft Fuel Lines," *Fuel* 254 (2019): 115616, https://doi.org/10.1016/j.fuel.2019.115616.
18. Schmitz, M. and Schmitz, G., "Experimental Study on the Accretion and Release of Ice in Aviation Jet Fuel," *Aerosp. Sci. Technol.* 82-83 (2018): 294-303, https://doi.org/10.1016/j.ast.2018.08.034.
19. Zhang, W., Webb, D.J., Carpenter, M., and Williams, C., "Measuring Water Activity of Aviation Fuel Using a Polymer Optical Fiber Bragg Grating," 2014, https://doi.org/10.1117/12.2059273.
20. Zhang, C., Chen, X., Webb, D.J., and Peng, G.-D., "Water Detection in Jet Fuel Using a Polymer Optical Fibre Bragg Grating," in *20th International Conference on Optical Fibre Sensors*, 2009, 750380, https://doi.org/10.1117/12.848696.
21. McClain, S.T., Zhang, T., Ahmed, S.U., Stafford, G. et al., "A Climatic Facility and Apparatus for Investigations of Cold Soaked Fuel Frost Evolution," in *AIAA Aviat. 2020 Forum*, 2020, https://doi.org/10.2514/6.2020-2808.
22. Clark, A.Q., Smith, A.G., Threadgold, S., and Taylor, S.E., "Dispersed Water and Particulates in Jet Fuel: Size Analysis under Operational Conditions and Application to Coalescer Disarming," *Ind. Eng. Chem. Res.* 50 (2011): 5749-5765, https://doi.org/10.1021/ie102533e.
23. Thompson, A.B. and Lam, J.K.W., "Water Run-Off in Aircraft Fuel Tanks," *IMA J. Appl. Math. (Institute Math. Its Appl.)* 77 (2012): 72-85, https://doi.org/10.1093/imamat/hxr077.
24. Charro, A., Baena, S., and Lam, J.K., "Water Solubility in Different Alternative Jet Fuels: A Comparison with Petroleum-Based Jet Fuel," SAE Technical Paper 2015-01-2563, 2015, https://doi.org/10.4271/2015-01-2563.
25. Elliott, J.W. and Smith, F.T., "Ice Formation on a Smooth or Rough Cold Surface due to the Impact of a Supercooled Water Droplet," *J. Eng. Math.* 102 (2017): 35-64, https://doi.org/10.1007/s10665-015-9784-z.
26. Miller, A.J., Brennan, K.P., Mignani, C., Wieder, J. et al., "Development of the Drop Freezing Ice Nuclei Counter (FINC), Intercomparison of Droplet Freezing Techniques, and Use of Soluble Lignin as an Atmospheric Ice Nucleation Standard," *Atmos. Meas. Tech.* 14 (2021): 3131-3151, https://doi.org/10.5194/amt-14-3131-2021.
27. Bernstein, B.C., Wolff, C.A., and McDonough, F., "An Inferred Climatology of Icing Conditions Aloft, Including Supercooled Large Drops. Part I: Canada and the Continental United States," *J. Appl. Meteorol. Climatol.* 46 (2007): 1857-1878, https://doi.org/10.1175/2007JAMC1607.1.

28. Bernstein, B.C. and Le Bot, C., "An Inferred Climatology of Icing Conditions Aloft, Including Supercooled Large Drops. Part II: Europe, Asia, and the Globe," *J. Appl. Meteorol. Climatol.* 48 (2009): 1503-1526, https://doi.org/10.1175/2009JAMC2073.1.
29. Xu, Y., Petrik, N.G., Smith, R.S., Kay, B.D. et al., "Homogeneous Nucleation of Ice in Transiently-Heated, Supercooled Liquid Water Films," *J. Phys. Chem. Lett.* 8 (2017): 5736-5743, https://doi.org/10.1021/acs.jpclett.7b02685.
30. Goodarzi, F. and Zendehboudi, S., "A Comprehensive Review on Emulsions and Emulsion Stability in Chemical and Energy Industries," *Can. J. Chem. Eng.* 97 (2019): 281-309, https://doi.org/10.1002/cjce.23336.
31. Bessee, G., "Determination of Water Droplet Size Distributions in Diesel and Aviation Fuels," in *13th International Conference on Stability, Handling and Use of Liquid Fuels 2013*, 2013, 267-272.
32. Zschocke, A., Scheuermann, S., and Ortner, J., "High Biofuel Blends in Aviation (HBBA)," Interim Report, ENER C. 2, 2017, 420-421.
33. Holladay, J., "Review of Technical Studies," 2020, 1-4.
34. Pray, T., Pramanik, J., McPhee, D., Galazzo, J. et al., "Integrated Biorefinery Operations for Domestic Renewable Diesel and Chemical Production," in: *Proceedings of the 32nd Symposium on Biotechnology for Fuels and Chemical*, Clearwater Beach FL, 2010.
35. Wedd, M., "Particle Size Analysis," in *Encyclopedia of Analytical Science*, 2nd ed. (Amsterdam: Elsevier, 2004), 18-29, https://doi.org/10.1016/B0-12-369397-7/00439-8.
36. ISO 9276-2:2014, "Representation of Results of Particle Size Analysis—Part 2: Calculation of Average Particle Sizes/Diameters and Moments from Particle Size Distributions," 2014, https://www.iso.org/standard/57641.html.
37. Westfall, P.H., "Kurtosis as Peakedness, 1905-2014. 'R.I.P.'," *Am. Stat.* 68 (2014): 191-195, https://doi.org/10.1080/00031305.2014.917055.
38. Wang, F., Liu, R., Li, M., Yao, J. et al., "Kerosene Evaporation Rate in High Temperature Air Stationary and Convective Environment," *Fuel* 211 (2018): 582-590, https://doi.org/10.1016/j.fuel.2017.08.062.
39. Ugbeh, J., Carpenter, M., and Pons, J., "Assessment of HEFA, ATJ, GTL S-8 and Farnesane as Alternative Jet Fuels Based on Their Water Shedding Characteristics," in *Proceedings of the 16th International Conference on Stability and Handling of Liquid Fuels*, 2019, https://iash.conferencespot.org/69070-iash-1.4569809/t001-1.4569870/f0015-1.4569871/a073-1.4569883/ap214-1.4569886?qr=1.
40. Ragab, A.M., "Water-in-Diesel Fuel Nanoemulsions: Preparation, Stability, Rheological and Physical Properties," *J. Pet. Environ. Biotechnol.* (2014), https://doi.org/10.4172/2157-7463.s1.008.
41. Noor El-Din, M.R., El-Hamouly, S.H., Mohamed, H.M., Mishrif, M.R. et al., "Water-in-Diesel Fuel Nanoemulsions: Preparation, Stability and Physical Properties," *Egypt. J. Pet.* 22 (2013): 517-530, https://doi.org/10.1016/j.ejpe.2013.11.006.
42. Leiva, J.M. and Geffroy, E., "Evolution of the Size Distribution of an Emulsion under a Simple Shear Flow," *Fluids* 3 (2018): 46, https://doi.org/10.3390/fluids3030046.

Appendix A

TABLE A.1 KF experimental data for neat fuels with 1000 ppm nominal water addition.

Conv. Jet A-1		100% SASOL		100% GTL	
TI (min)	KF water content (ppm)	TI (min)	KF water content (ppm)	TI (min)	KF water content (ppm)
1	1078	1	991	1	996
2	1009	2	767	2	798
5	975	5	678	5	729
32	889	32	522	32	559
34	884	34	525	34	581
60	782	60	529	60	544
62	789	62	522	62	531
100% HEFA		**100% ATJ**		**100% Farnesane**	
TI (min)	KF water content (ppm)	TI (min)	KF water content (ppm)	TI (min)	KF water content (ppm)
1	1029	1	1019	1	1199
2	829	2	995	2	1186
5	837	5	931	5	1119
32	859	32	855	32	1001
34	849	34	856	34	1015
60	767	60	427	60	991
62	777	62	439	62	989

Appendix B

The droplet frequency distribution for all Cases a.1-a.6 is given in Figure B.1. This reveals that the droplet counts are separated into discrete size intervals between Jet A-1 fuel and sustainable aviation fuels explored for this work. The height of the rectangular bar/peak indicates the total count of water droplets in each range. If the magnitudes of the rectangular bars for the different size intervals are summed, it will give the total droplet count of the selected fuel.

FIGURE B.1 Frequency distribution of the different size water droplets after 100 min settling for the six aviation fuels explored in this work.

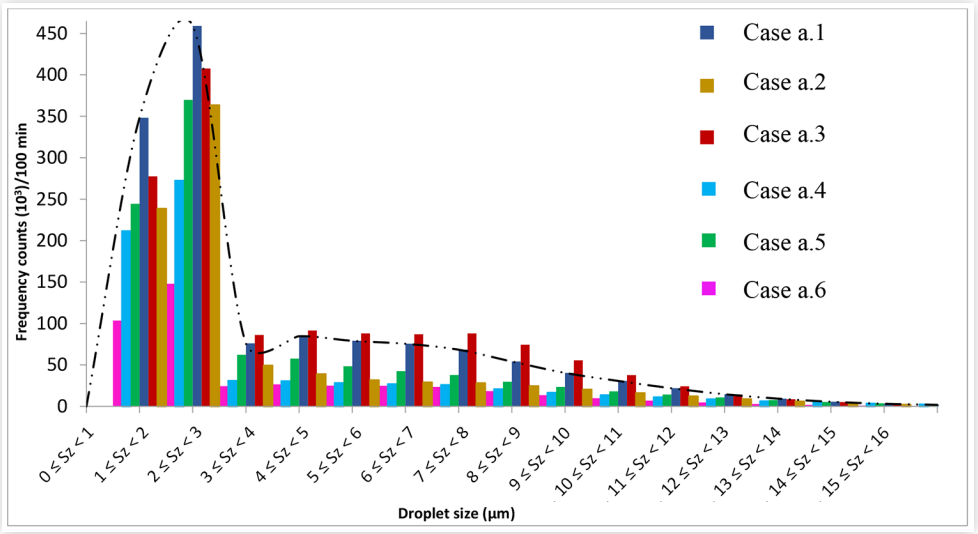

Appendix C

Figure C.1 shows the corresponding water droplet size population against time for all Cases a.1-a.6 tests and hexanol. The droplet size population for hexanol was also included to serve as the baseline for extreme comparison between a stable solution and unstable solution for data clarity, as hexanol is likely to form a very stable solution.

The minimal change seen for hexanol, and Case a.6, can be attributed to the fact that a highly stable solution was formed. This means there exists a good mix between the water fuel mixture. The noticeable gap between d90-d50 water droplets and d40-d10 droplets can be attributed to a lesser frequency/count distribution of the larger droplets in comparison to that of the smaller droplets (d40-d10).

FIGURE C.1 (a.1-a.6) Water droplet size population represented against time for Test cases a.1-a.6; a.1′-a.6′ shows an indication that coalescence occurred.